


Interannual-to-decadal variability and trends of sea level in the South China Sea

Xuhua Cheng¹  · Shang-Ping Xie^{2,3} · Yan Du¹ · Jing Wang⁴ · Xiao Chen¹ · Juan Wang⁴

Received: 23 June 2014 / Accepted: 4 July 2015 / Published online: 17 July 2015
© Springer-Verlag Berlin Heidelberg 2015

Abstract Interannual-to-decadal variability and trends of sea level in the South China Sea (SCS) are studied using altimetric data during 1993–2012 and reconstructed sea level data from 1950–2009. The interannual variability shows a strong seasonality. Surface wind anomalies associated with El Niño–Southern Oscillation explain the sea-level anomaly pattern in the interior SCS, while Rossby waves radiated from the eastern boundary dominate the sea-level variability in the eastern SCS. Decadal variability of sea level in the SCS follows that in the western tropical Pacific, with large variance found west of Luzon Island. Local atmospheric forcing makes a negative contribution to decadal variability in the central SCS, and Rossby waves radiated from the eastern boundary appear to be important. During 1993–2012, decadal sea level averaged in the SCS is significantly correlated with the Pacific Decadal Oscillation (PDO) ($r = -0.96$). The decadal variability associated with the PDO accounts for most part of sea-level trends in the SCS in the last two decades.

Keywords Sea level · Interannual and decadal variability · Altimetric data · Rossby waves · Pacific Decadal Oscillation

1 Introduction

1.1 Background

The South China Sea (SCS) is the largest semi-enclosed marginal sea in the northwest Pacific, connecting to the Java and Sulu Seas through a number of shallow passages in the south and to the Pacific through the deep Luzon Strait in the north (Fig. 1). Sea level varies in the SCS at interannual-to-decadal timescales (e.g., Wu and Chang 2005; Fang et al. 2006; Cheng and Qi 2007; Peng et al. 2013).

Interannual sea-level variability in the SCS has been investigated in a number of studies (e.g., Wu and Chang 2005; Fang et al. 2006; Rong et al. 2007; Chang et al. 2008; Liu et al. 2011; Peng et al. 2013). Wu and Chang (2005) analyzed 10-year sea-surface-height data from a data-assimilation model using empirical orthogonal functions (EOFs). They found that the first and second modes dominate the interannual variations in winter and summer, respectively, with both modes being highly correlated with El Niño–Southern Oscillation (ENSO). Using satellite observations, Fang et al. (2006) found that the first EOF of sea level is characterized by high sea-level variability along the eastern boundary of the SCS. The corresponding principal component is highly correlated with the Niño3.4 sea-surface temperature anomaly (SSTa) index (SSTa anomaly averaged in 5°S–5°N, 170°W–120°W), with the correlation coefficient reaching a maximum (0.94) when the sea-level principal component lags ENSO by 2 months. Based on altimetric data during 1993–2004, Rong et al. (2007)

✉ Xuhua Cheng
xuhuacheng@scsio.ac.cn

¹ State Key Laboratory of Tropical Oceanography, South China Sea Institute of Oceanology, Chinese Academy of Sciences, 164 West Xingang Road, 510301 Guangzhou, China

² Scripps Institution of Oceanography, University of California at San Diego, La Jolla, CA 92093-0206, USA

³ Physical Oceanography Laboratory, Qingdao Collaborative Innovation Center of Marine Science and Technology, Ocean University of China, Qingdao, China

⁴ School of Geography and Planning, Sun Yat-sen University, Guangzhou, China

reported that SCS sea level decreases (increases) during El Niño (La Niña) events.

Some studies have suggested the importance of wind forcing in explaining the sea-level patterns revealed by EOF analysis (e.g., Wu and Chang 2005; Fang et al. 2006; Chang et al. 2008). Further, previous studies found that sea-level variations along the west coast of the Luzon Island are modulated by signals from the western tropical Pacific (WTP), but they did not discuss how these signals affect sea level in the interior SCS (Liu et al. 2011; Zhuang et al. 2013b; Chen et al. 2015). The contributions of both local wind forcing and remote forcing from the western Pacific to SCS sea level needs to be quantified.

Several studies have investigated the long-term sea-level change in the SCS (e.g., Li et al. 2002; Fang et al. 2006; Rong et al. 2007; Peng et al. 2013). Li et al. (2002) found that the basin-mean sea level rose at a rate of about 10 mm/year during 1993–1999, and suggested that the increase is due to the upper ocean warming on decadal time scales. Fang et al. (2006) reported that SCS sea level rose at a rate of 6.7 ± 2.7 mm/year from 1993 to 2003, while Peng et al. (2013) found a rate of 3.9 ± 0.6 mm/year based on satellite altimetric data during 1993–2009. Over 1993–2012, sea level trends in subregions of the SCS range from 1–8 mm/year, with a basin-mean value of about 5.0 mm/year (Fig. 1).

The above studies were based on short record lengths of altimetry data and could be detecting decadal-to-interdecadal variability of sea level in the SCS. Cheng and Qi (2007) revealed a significant decadal phase shift in SCS sea level over 1993–2005, which is very similar to that in the western Pacific (Cheng et al. 2008; Lee and McPhaden 2008). A number of studies have suggested that a significant part of the interdecadal variability and decadal trend of sea level in the WTP may be related to the Pacific Decadal

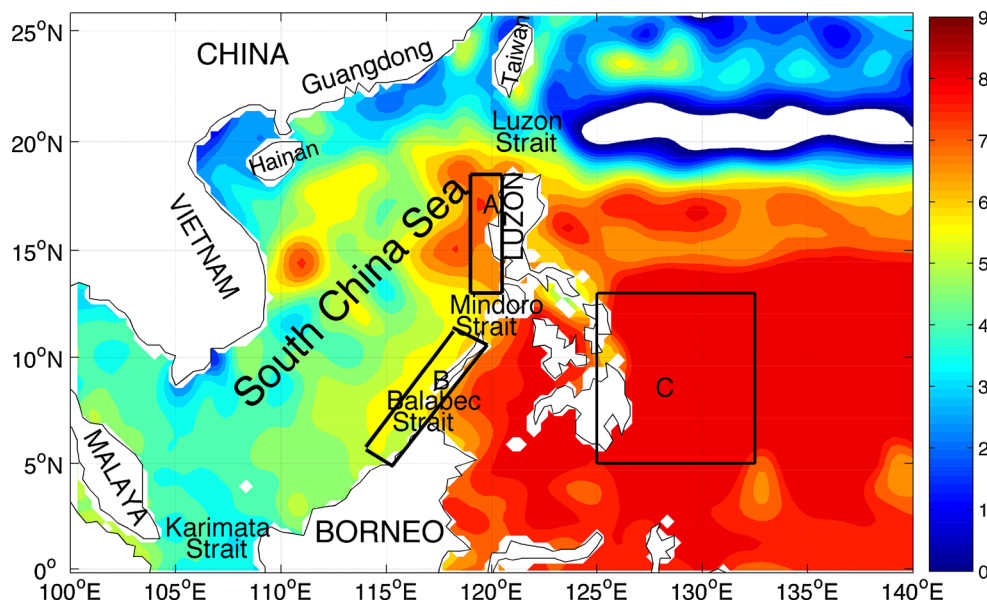
Oscillation (PDO) or the Indian Ocean warming in recent decades (e.g., Du and Xie 2008; Merrifield et al. 2012; Luo et al. 2012; Zhang and Church 2012; Han et al. 2013). So far, the decadal variability of sea level in the SCS and its relation with the PDO has not been systematically investigated. To study the decadal variability, it is helpful to isolate the contribution of climate mode to sea-level trends in the SCS for the satellite altimetry era.

1.2 Present research

In this study, we continue the effort to identify characteristics of interannual and decadal sea-level variability in the SCS. Our approach is to analyze the longer data records that are now available: Altimetric data have accumulated for more than 20 years, and several reconstructed sea-level products are available (e.g., Church and White 2006; Hamlington et al. 2011). In addition, we obtain solutions to an ocean model in order to isolate the key mechanisms that forced the variability.

Associated with ENSO events, interannual variability of sea level in the SCS is season-dependent. In previous studies, the seasonality of interannual events has been largely ignored. We show that the interannual variability of sea level in the SCS has seasonally distinct patterns. In the interior of the SCS, sea-level variability can be explained by wind anomalies, whereas in the eastern basin Rossby waves radiated from the eastern boundary are most important. The decadal variability of sea level in the SCS is forced by that in the western Pacific, and highly correlated with the PDO. Westward-propagating Rossby waves radiated from the eastern boundary dominate the decadal variability of sea level in the SCS, whereas winds forcing tend to dampen the decadal signal in the central SCS. The decadal variability

Fig. 1 Sea-level trends (mm/year) over the South China Sea derived from altimetric data during 1993–2012



associated with PDO accounts for most part of sea-level trends in the SCS from 1993–2012.

The rest of the paper is organized as follows. Section 2 describes the datasets and methods used for the analysis. Section 3 studies the interannual and decadal variability of sea level in the SCS and the physical mechanisms. Section 4 presents conclusions with discussions.

2 Data and methods

2.1 Data sets

The sea-level anomaly (SLA) data used in this study are taken from the Archiving, Validation and Interpretation of Satellite Oceanographic (AVISO, <http://www.aviso.oceanobs.com/>) data set, a merged product determined from multiple satellite missions (T/P and ERS-1/2, followed by Jason-1/2 and Envisat). The aliasing of tides and barotropic variability have been removed using tidal model GOT2000 and the barotropic hydrodynamic model MOG2D-G (Volkov et al. 2007; Dibarboure et al. 2008). The product is available on a 1/3° Mercator grid at weekly intervals and spans a period from 1993 to 2012.

To examine sea-level change over periods longer than can be resolved with satellite observations, we used reconstructed sea-level data from 1950 to 2009 (Hamlington et al. 2011, hereafter H2011). The reconstructed data are obtained by utilizing cyclostationary empirical orthogonal functions (CSEOFs) derived from satellite altimetry and historical sea-level measurements from tide gauges. CSEOFs are able to extract cyclostationary signals in a single mode, which has significant advantages compared with EOFs when analyzing annual cycle and ENSO signals (Hamlington et al. 2011).

Thermosteric sea level is significant correlated with sea level in the SCS and western Pacific (Cheng and Qi 2007; Cheng et al. 2008), and hence provides a useful substitute for the total sea level in this region (Nidheesh et al. 2012; Han et al. 2013). We use the Ishii dataset to reveal decadal variability of thermosteric sea level change during 1950–2011 (Ishii et al. 2006; Ishii and Kimoto 2009).

We used the formula proposed by Wu (1982) to calculate surface wind stress using EAR-Interim monthly sea surface wind speed data from the European Centre for Medium-Range Weather Forecasts (ECWMF) product. The data is available on a 0.75° × 0.75° grid (Dee et al. 2011; <http://www.ecmwf.int/products/data/archive/>).

2.2 Ocean model

Previous studies have indicated that sea-level variability in the open ocean can be largely explained by the

westward-propagating baroclinic Rossby waves, which are driven by wind stress curl and/or radiated from the eastern boundary (Fu and Qiu 2002; Qiu 2002; Wang et al. 2010; Zhuang et al. 2013a; Wang et al. 2015). To examine the effect of forcing by interior winds and Rossby waves from the eastern boundary of the SCS, we obtained solutions to a 1.5-layer (reduced-gravity) model. The model, which contains the simple dynamics of a wind-forced upper-ocean layer, has been used in the study of upper-ocean circulation, sea-level fluctuations, and mesoscale eddies in the SCS (e.g., Metzger and Hurlbert, 1996; Liu et al. 2001; Wang et al. 2006, 2010; Zhuang et al. 2013b).

Following Qiu (2002), the long-wave equation governing sea level is

$$\frac{\partial h}{\partial t} - C_R \frac{\partial h}{\partial x} = -\frac{g' \nabla \times \tau}{\rho_0 g f} - \varepsilon h \tag{1}$$

where h is baroclinic component of the sea level, C_R the phase speed of long baroclinic Rossby waves, τ the wind stress, and ε the Newtonian damping. Other variables are time (t), longitudinal coordinate (x), the Coriolis parameter (f), gravitational constant (g), reduced-gravity coefficient (g'), and background density (ρ_0).

The solution is obtained by integrating (1) westward from the eastern boundary (x_e) to get

$$h(x, y, t) = h\left(x_e, y, t + \frac{x - x_e}{C_R}\right) \exp\left[\frac{\varepsilon}{C_R}(x - x_e)\right] + \frac{1}{\rho_0 g f} \int_{x_e}^x \frac{g'}{C_R} \nabla \times \tau\left(x', y, t + \frac{x - x_e}{C_R}\right) \times \exp\left[\frac{\varepsilon}{C_R}(x - x_e)\right] dx' \tag{2}$$

The first term on the right-hand side of (2) represents the influence of sea-level signals propagating from the eastern boundary as a packet of Rossby waves, whereas the second specifies the response due to interior wind forcing.

In evaluating (2), we set $g' = 0.03 \text{ m/s}^2$ (Liu et al. 2001). Following Liu et al. (2001) and Fu and Qiu (2002), the wave speed of the first baroclinic long Rossby wave is defined as $C_R = -\beta g' H_e / f^2$, except at some latitudinal bands where it is determined from altimetric observations. $\beta = f_y$ is the meridional gradient of f and is the equivalent depth of the model. The dissipation rate ε varies from $(2 \text{ year})^{-1}$ in the northern shelf to $(0.5 \text{ year})^{-1}$ in the southern SCS. The eastern-boundary sea level, $h(x_e, y, t)$ is determined by the monthly altimetric SLA in the grid cells closest to the eastern boundary, with the climatological monthly mean and intraseasonal signals (<3 month) removed. In the Luzon Strait, we take the eastern boundary to be along 120.5°E, which includes impacts from the Pacific. Wind stress curl is calculated using wind stress derived from EAR-Interim sea surface wind speed.

Fig. 2 Time-longitude plot of the sea-level anomalies (period > 1 year, cm) averaged along 17–18°N latitudinal band from **a** altimetric observations, and **b** the 1.5-layer model

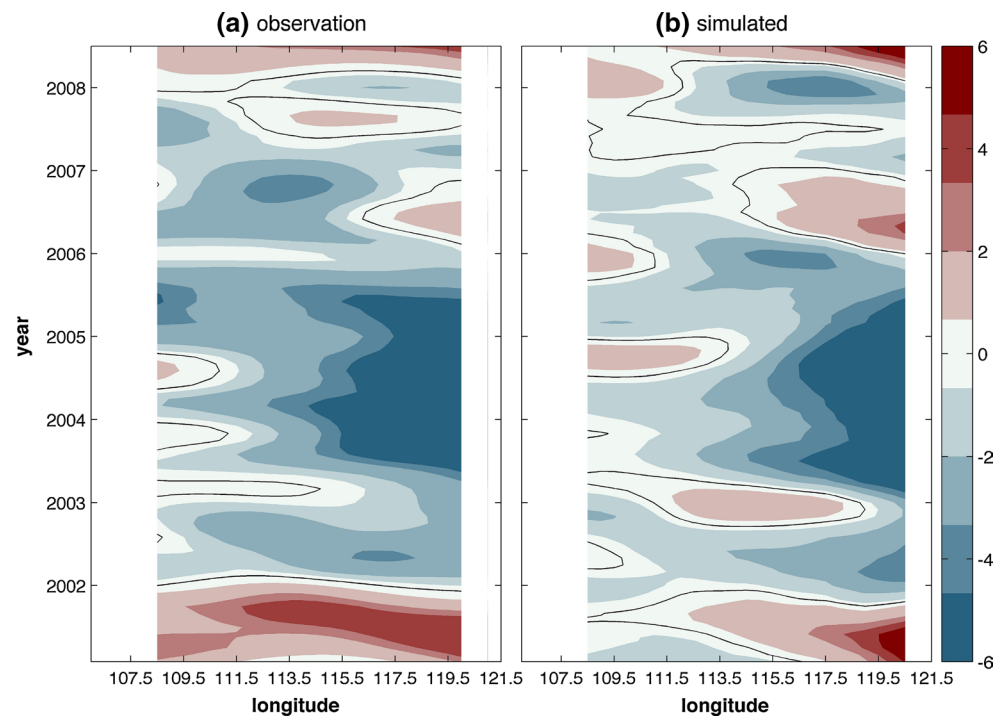


Figure 2 shows time-longitude diagrams of observed and modeled low-frequency SLA averaged from 17–18°N. Both observed and simulated SLA show significant westward extension. In addition to the good agreements near the eastern boundary, sea-level signals in the west also match quite well. Figure 3 shows the point-to-point correlation coefficient between sea level from satellite observations and 1.5-layer reduced gravity model during 1995–2012. Significant correlations are found in whole deep basin ($r > 0.5$), indicating the capability of the model to simulate large-scale and low frequency sea-level fluctuations in the SCS.

2.3 Analyses

Our analyses all use monthly mean data, from which anomalies are calculated by subtracting their climatological monthly means. The anomaly data are then smoothed in time using a 3-month running mean to remove intraseasonal signals.

Power spectra for H2011 and OFES sea level averaged in the SCS show two broad spectral peaks. One peaks at 2–7 and the other peaks at 7–15 year (Fig. 4a), representing interannual and decadal variability, respectively. The power spectra determined from satellite data is similar, except with a weaker decadal band due to the shorter record (Fig. 4b). We separate signals into interannual and decadal bands by high-passing (periods < 7 year) and low-passing (periods > 7 year) them, respectively. Note that, because the lower bound of the interannual band is 3 months, it can

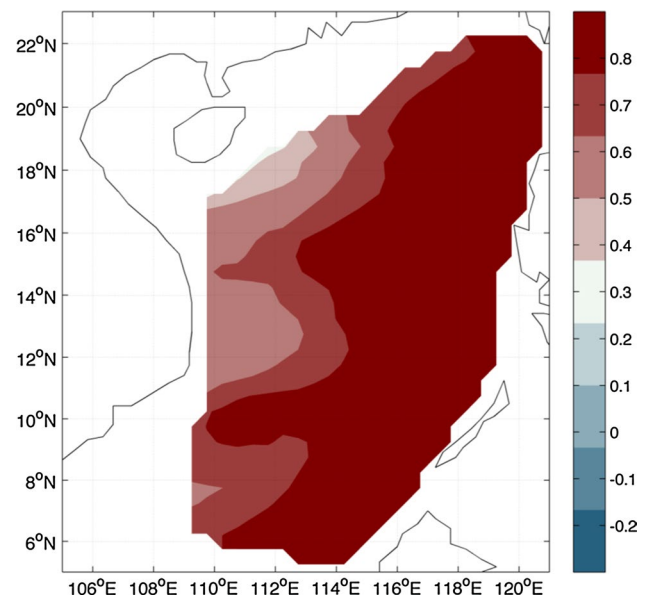
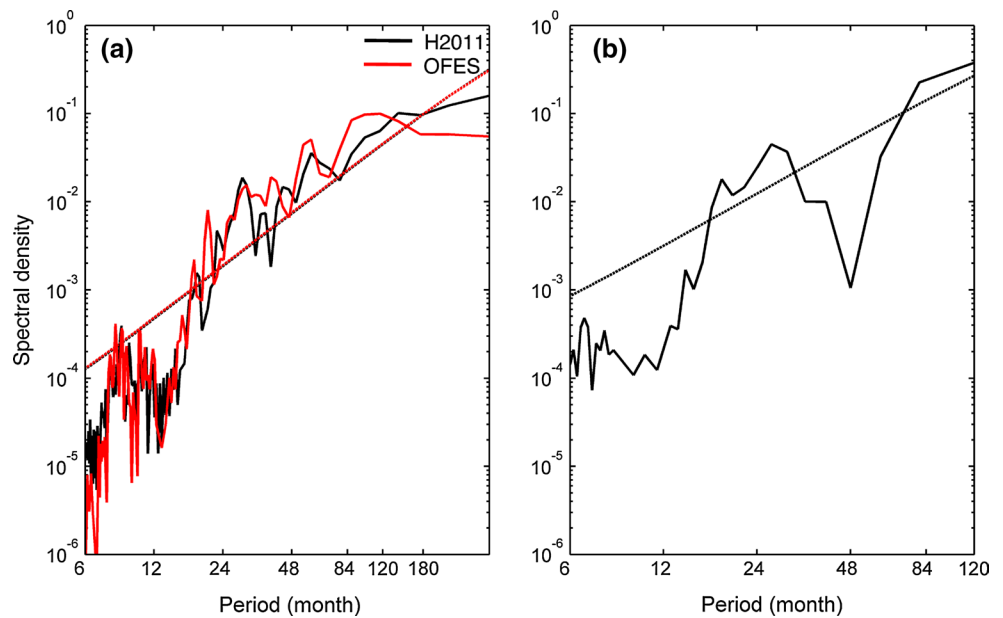


Fig. 3 Point-to-point correlation coefficient between low-frequency sea level from satellite observations and 1.5-layer reduced gravity model during 1995–2012

be used to examine the seasonality of interannual events like ENSO.

We utilize a seasonal-reliant empirical orthogonal function (S-EOF) analysis to extract major modes of sea-level and wind-field variability during ENSO events. The S-EOF technique reveals the evolution of a particular mode with reference to the annual cycle (Wang and An 2005).

Fig. 4 **a** Power spectra for reconstructed and OFES sea level anomaly averaged in the SCS (105–121°E, 5–23°N). The 95 % confidence level is shown by dashed line. The timeseries are smoothed using a 13-month running mean to remove signals with periods shorter than 1 year. **b** As in (a), except for altimetric observations



We use a multiple variable linear regression (MVLRL) for 1993–2012 to isolate the impact of PDO on long-term trend of sea level (Zhang and Church 2012):

$$y = a_0 + a_1t + a_2PDO + \varepsilon_a. \tag{3}$$

where y is the SLA in the SCS, a_1 is the linear trend derived from the MVLRL, a_2 is the regression coefficient with respect to the PDO index, and ε_a is the error.

3 Results

3.1 Interannual variability

3.1.1 Seasonality

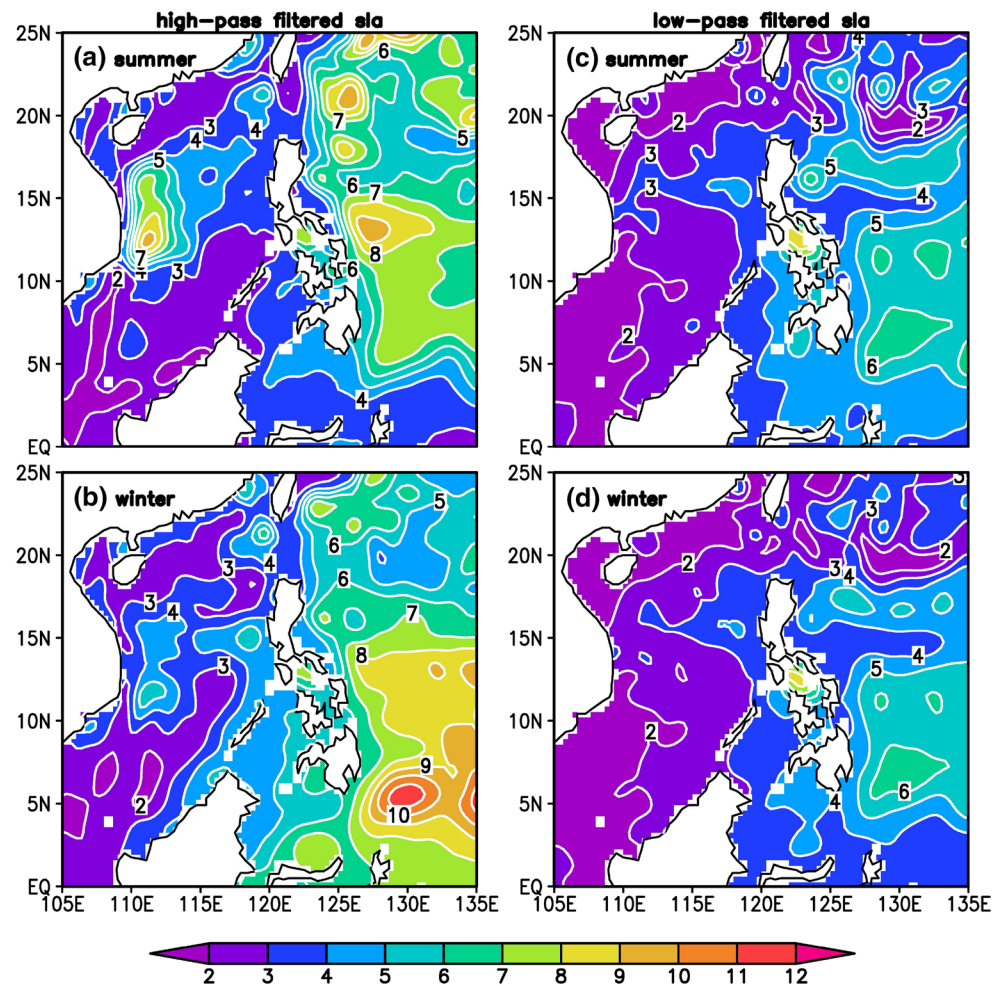
On interannual time scales, the atmosphere–ocean system over the Indo-Pacific warm pool region is strongly modulated by ENSO events (e.g., Wang et al. 2000; Lau and Wang 2005; Xie et al. 2009). Their effects on the seasonal variability of wind, precipitation, sea surface temperature, and sea level pressure in the SCS have been previously discussed. Here, we discuss how they affect sea level.

Figure 5a shows the standard deviation (STD) of interannual SLA during summer. In the SCS, high STD is located east of Vietnam, with a maximum of 9 cm, there is another high west of Luzon Strait, and STD is weakest in the southern SCS. During the winter (Fig. 5b), SLA shows high value along the coast and east of Vietnam, and relatively weak variance in the southern SCS (Fig. 5b). A comparison of Fig. 5a, b shows that the interannual variability of sea level has significant seasonality.

Figure 6a–d plots the first S-EOF mode of sea level from the winter during an ENSO event to the following fall. The different months are denoted by D(0)JF(1), MAM(1), JJA(1) and SON(1). The first mode accounts for 24 % of the total variance of the interannual signal. During El Niño developing winters, the first sea-level mode is characterized by negative anomalies along the southeast and north coasts and positive anomalies in the deep basin (Fig. 6a, i). During El Niño decaying summers, it has positive anomalies in the central basin with westward intensification, which lies between negative anomalies to the north and south (Fig. 6c, i). Spring and fall are transition seasons between the monsoons, with weaker wind anomalies. The S-EOF pattern in MAM(1) (SON(1)) is similar to that in winter (summer) (Fig. 6b, d). The correlation coefficient between PC1 and the D(0) JF(1) Niño3.4 index is 0.86 (Fig. 6i), which is significant at the 99 % level, demonstrating that mode 1 is caused by ENSO. It is noteworthy that the SLA pattern during summer revealed by the S-EOF is opposite to that in the study of Wu and Chang (2005). They revealed a SLA pattern during El Niño developing summers, which has a significant correlation with ENSO when it leading Niño3.4 index by 3 months. But in this study, sea level variability during El Niño decaying summers is presented, which has a significant correlation with Niño3.4 index by lagging 6 months.

The PC1 of wind stress curl has a significant correlation with ENSO ($r = 0.89$). During El Niño events (such as 1997/1998 and 2009/2010), surface wind anomalies in D(0) JF(1) are anticyclonic (Fig. 6e), which potentially drives positive SLA in the deep basin and negative SLA along the western and northern coastal regions (Fig. 6a). The reverse is true during La Niña events (such as 1999–2001,

Fig. 5 **a** Standard deviation of interannual sea-level anomalies during summer (cm), **b** Same as (a) but for winter. **c, d** Same as (a) and (b), but for decadal sea-level anomalies



2008/2009 and 2010/2011). In the summer following an El Niño event, the surface wind in the SCS features an anticyclonic anomaly in the central SCS and a cyclonic anomaly in the southern SCS (Fig. 6g), with a weakened southwest summer monsoon. The SCS wind anomalies are part of a larger-scale anticyclone that develops during the summer following El Niño from the Northwest Pacific to North Indian Ocean, a phenomenon called the Indian-Ocean capacitor effect (Yang et al. 2007; Xie et al. 2009, 2010). These wind anomalies drive positive SLA in the central basin and negative SLA in the southern SCS. The Indian Ocean capacitor effect has been applied to explain the interannual variability of summer coastal upwelling in the SCS and cyclones in the tropical northwestern Pacific (Xie et al. 2003; Du et al. 2011; Jing et al. 2011). Figure 6c, g suggest that this theory can also be used to explain the summer SLA.

3.1.2 Model simulations

Figure 6 demonstrates that the interannual SLA pattern in the SCS is linked to the wind forcing associated with

ENSO. Since the transit of Rossby waves across the basin is rapid due to relatively small basin size of the SCS (Liu et al. 2001), we can therefore expect that SLA along the eastern boundary also affects the interior response. Here, we use a 1.5-layer reduced-gravity model to quantify the impacts of each contribution.

Figure 7a, b show the leading EOF patterns of interannual SLA due to wind-driven Rossby waves in the SCS (the second term on the right-hand side of Eq. 2). The winter EOF is characterized by positive SLA in the central basin and negative anomaly on the northern shelf, while the summer EOF features a dipole of positive anomalies to the north and negative anomalies to the south (Fig. 7b). The correlation coefficient between winter (summer) PC1 and the D(0)JF(1) Niño3.4 index is 0.87 (0.62), significant at the 95 % level.

The 1.5-layer model forced only by wind (top panels in Fig. 7) reproduces the main features of the observations, except for high negative anomalies along the eastern boundary (Fig. 6a). When Rossby waves from the eastern boundary (the first term on the right-hand side of Eq. 2) are also included, the negative anomaly in the eastern SCS

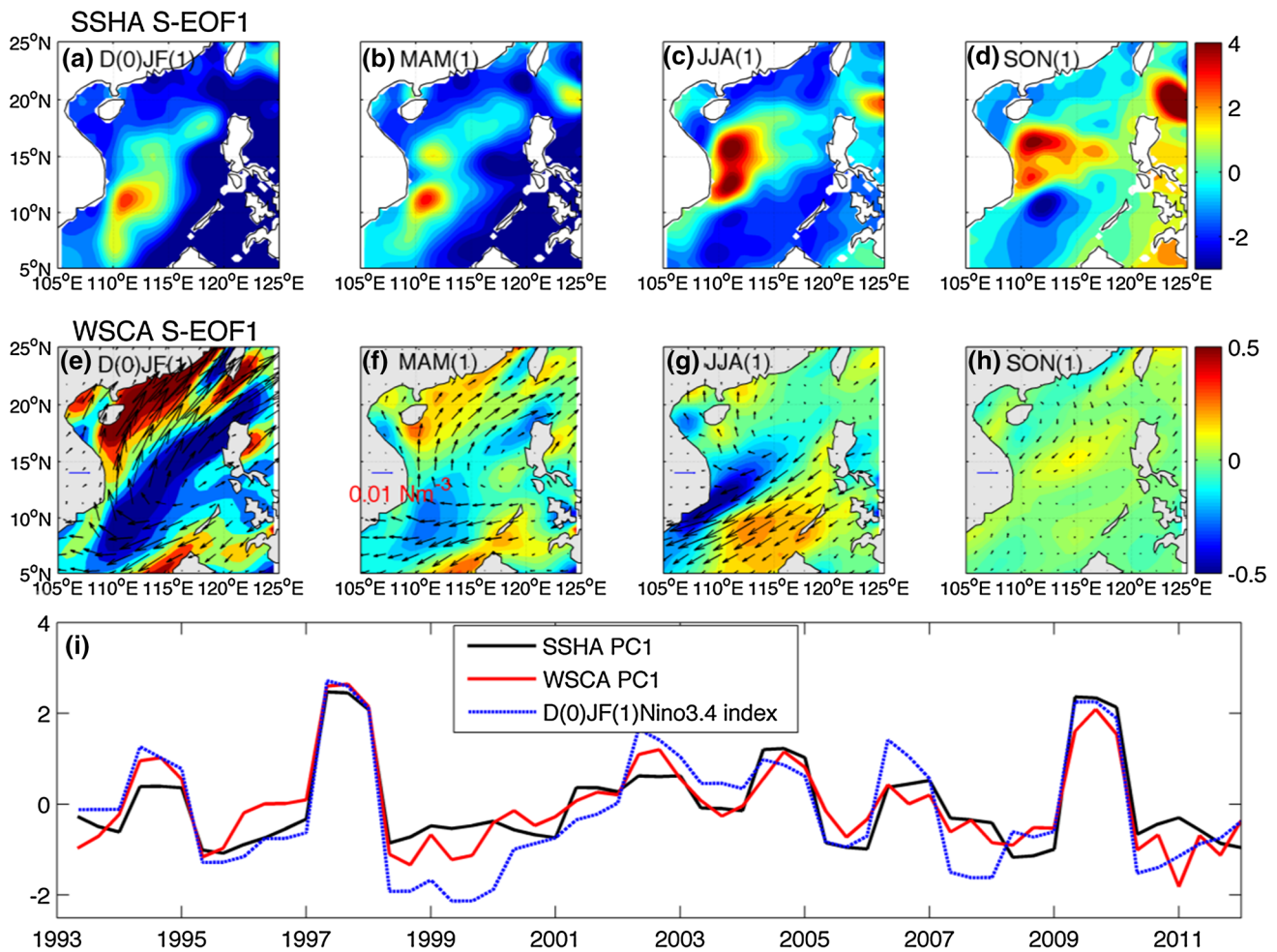


Fig. 6 a–d Spatial patterns of the first S-EOF mode of, showing the (D(0)JF(1)-to-SON(1)), interannual sea-level anomalies (cm) in the South China Sea. e–h Same as (a)–(d), except for the interannual wind-stress curl anomaly (shading, 10^{-7}N/m^3) and wind stress (vectors) derived from ERA-Interim reanalysis. i Normalized principal

component of the first S-EOF mode of (D(0)JF(1)-to-SON(1)), interannual sea level (black curve) and wind stress curl (red curve) anomalies. The dashed blue curve is the normalized D(0)JF(1) Nino3.4 index

is reproduced and the EOF patterns of SLA are in closer agreement with observations (Fig. 7c, d). Thus, the model results indicate that Rossby waves radiated from the eastern boundary are important in the eastern SCS, and act to weaken wind-driven sea level variability in the central SCS.

3.1.3 Origin of eastern-boundary signal

Since Rossby waves radiated from the eastern boundary play an important role in sea-level variations in the SCS, we examine the origin of the sea-level signals along the eastern boundary. Along the west coast of Borneo and Palawan Islands (box B in Fig. 1), correlation coefficient between the alongshore wind stress anomaly and SLA is 0.74 (significant at the 95 % level), indicating the importance of Ekman transport (Fig. 8b). In contrast, correlation between alongshore wind stress anomaly and SLA along the west

coast of Luzon Island (box A in Fig. 1) is not significant ($r = 0.15$). A significant correlation is found instead between SLA averaged in box A and that to the southeast of Philippine Archipelago (box C in Fig. 1, $r = 0.81$). Sea-level signals in the WTP can propagate into the SCS through the straits in the southeastern SCS, and then turn northward along the west coast of the Philippine Islands as trapped coastal waves (Fig. 9b). Due to the gap of Mindoro Strait, trapped coastal waves cannot propagate from the southeastern coast to the west coast of Luzon Island, as indicated by the abrupt decrease of lag correlation between stations 8 and 9 in Fig. 9c. So, sea-level fluctuation along the west coast of Luzon Island mainly originates from the WTP.

In the 1.5-layer model, observed sea level in the Luzon Strait is used as boundary condition, which includes the impact of Kuroshio and sea level signals from the Pacific.

Fig. 7 **a, b** First EOF patterns of interannual sea-level anomalies (cm) during winter and summer, forced by wind in the SCS. **c, d** Same as **(a)** and **(b)**, except for sea-level anomalies driven by the wind forcing and Rossby waves radiated from the eastern boundary of the SCS. The correlation (r) between the model PC and D(0)JF(1) Nino3.4 index is marked on each panel

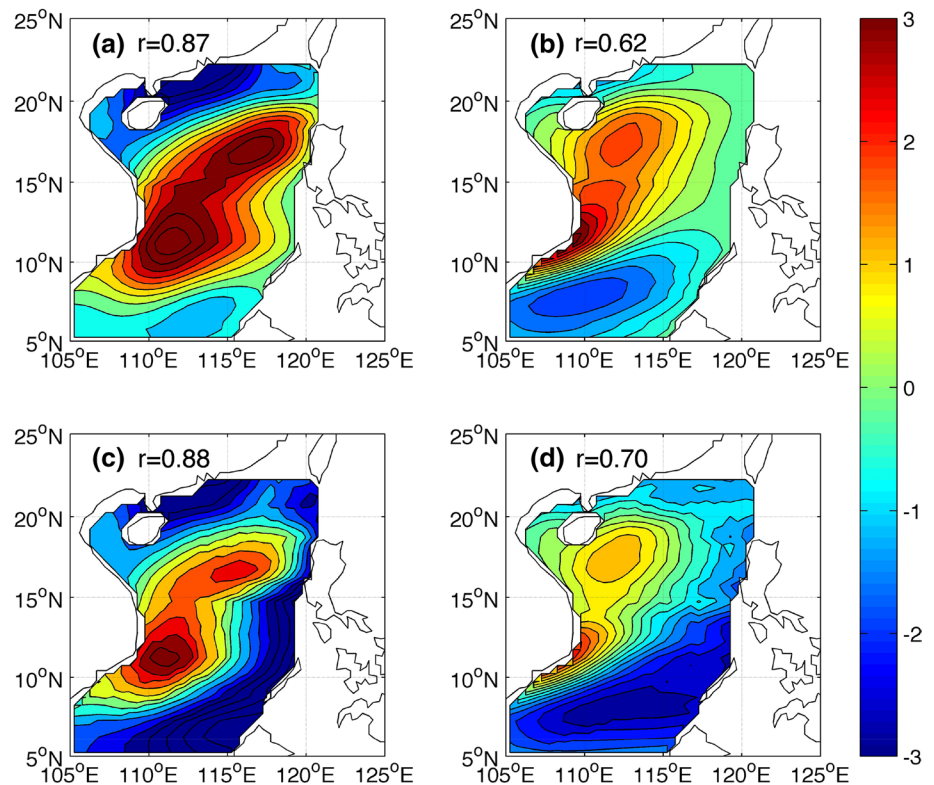
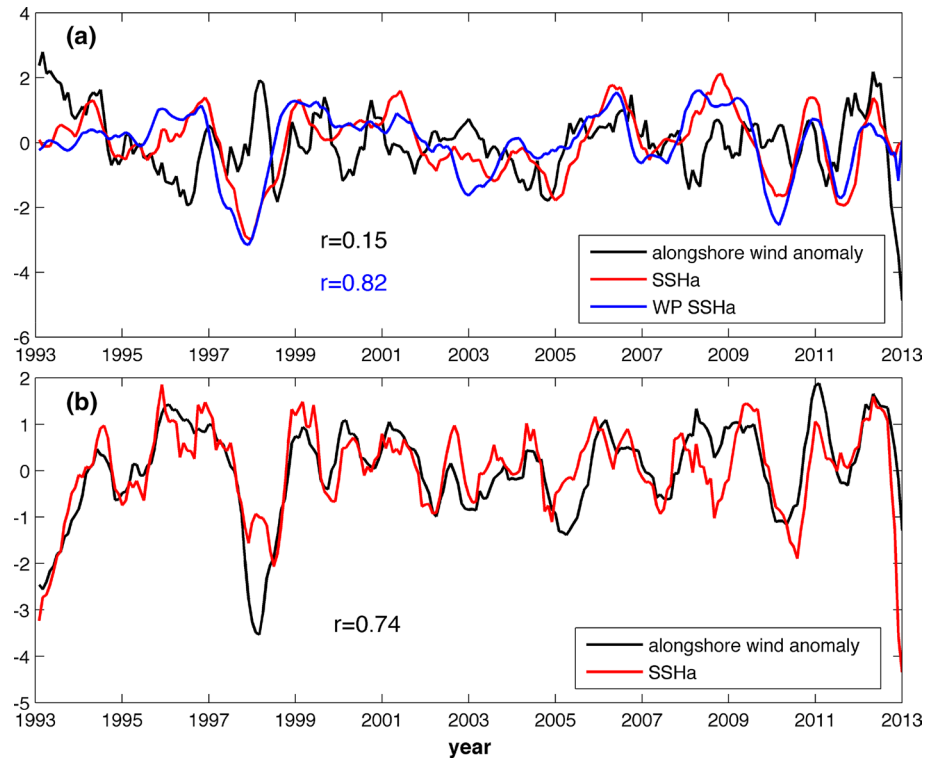


Fig. 8 **a** Time series of interannual SLA (red curve) and alongshore wind stress anomaly (black curve) averaged in region A (in Fig. 1), and SLA (blue curve) in the western Pacific in region C (in Fig. 1). **b** Time series of interannual SLA (red curve) and alongshore wind stress anomaly (black curve) averaged in region B. All time series are normalized by their respective standard deviations and have been detrended using linear least squares regression



How Kuroshio intrusions impact on sea-level variations in the SCS is beyond the scope of this study. Previous studies suggested Kuroshio intrusions through the Luzon Strait

not only affect the water properties, sea level and circulation in the SCS (Qu et al. 2000; Qu et al. 2006; Cheng and Qi 2007), but also convey the impact of ENSO and other

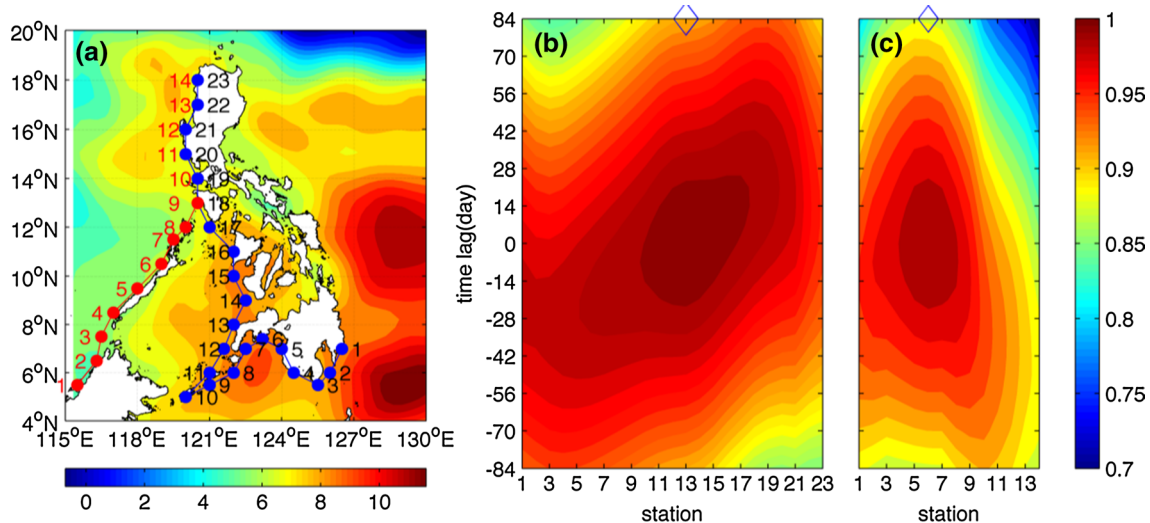


Fig. 9 **a** Sea level trends in the vicinity of Luzon Island derived from altimetric data during 1993–2012 (mm/year), superimposed on 1° boxes along two waveguide. **b** Time-station lag correlations of SLA from altimetric data along the west coast around the Philippine Archi-

pelago (blue points). SLA at station 13 is taken as the reference time series. **c** Time-station lag correlations of SLA from altimetric data along the eastern boundary of the SCS (red points). SLA at station 6 is taken as the reference time series

climate modes into the SCS (Qu et al. 2004; Du and Qu 2010; Gordon et al. 2012; Wu 2013; Yu and Qu 2013). Water entering the SCS through Luzon Strait is significantly cooler than that exiting through the Karimata and Mindoro Straits in the South. On interannual timescales, the westward Luzon Strait Transport (LST) increases (decreases) during El Niño (La Niña) events, inducing negative (positive) anomalies of basin-mean heat content and sea level in the SCS (Qu et al. 2004, 2006; Cheng and Qi 2007; Du and Qu 2010).

3.2 Decadal variability of sea level and its mechanism

3.2.1 Major features

Decadal, and longer, sea-level signals in the SCS, especially west of Luzon Island, exhibit a similar variability to that in the western Pacific (Fig. 5, panels c and d). Therefore, to consider the SCS and western Pacific as a whole is helpful to investigate the decadal sea level variability and possible mechanism in the SCS. Figure 10 displays the leading mode of decadal SLA in the SCS and western Pacific. The first mode accounts for 87 % of the total variance. Sea-level variability shows strong spatial coherence in this region. The highest variability is in the western Pacific from 5–20°N. In the SCS, relatively strong variability is found west of the Luzon Island. The PC1 shows distinct decadal variability, superimposed on a rising trend. Sea level in this region rose during 1995–2000, fell during 2001–2004, and then rose again during 2005–2012. The decadal variability has a significant

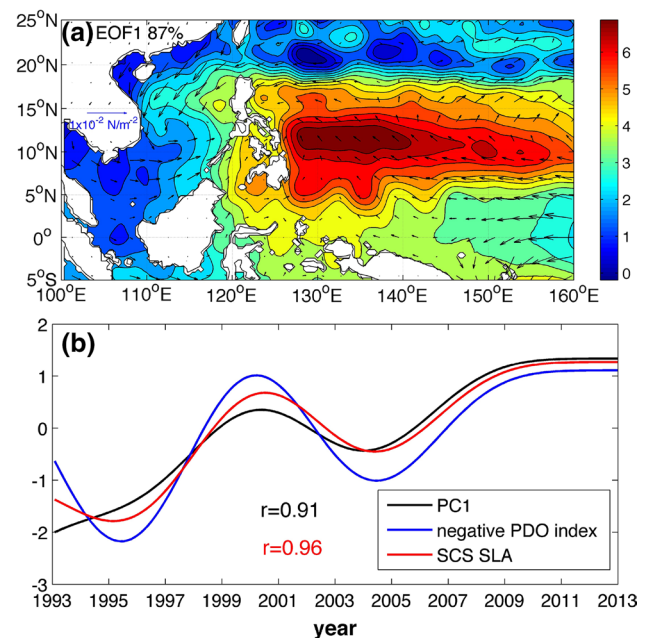


Fig. 10 **a** First EOF pattern of decadal sea level (cm) in the SCS and western Pacific, superimposed on regression coefficients of wind stress on the normalized negative PDO index. **b** Corresponding normalized principal component (black curve), normalized negative PDO index (blue curve) and normalized decadal mean sea level in the SCS (105–121°E, 5–23°N, red curve)

correlation with the negative PDO index ($r = 0.91$). The correlation coefficient between basin-mean decadal sea level over the SCS and the negative PDO index is 0.96 (Fig. 10b).

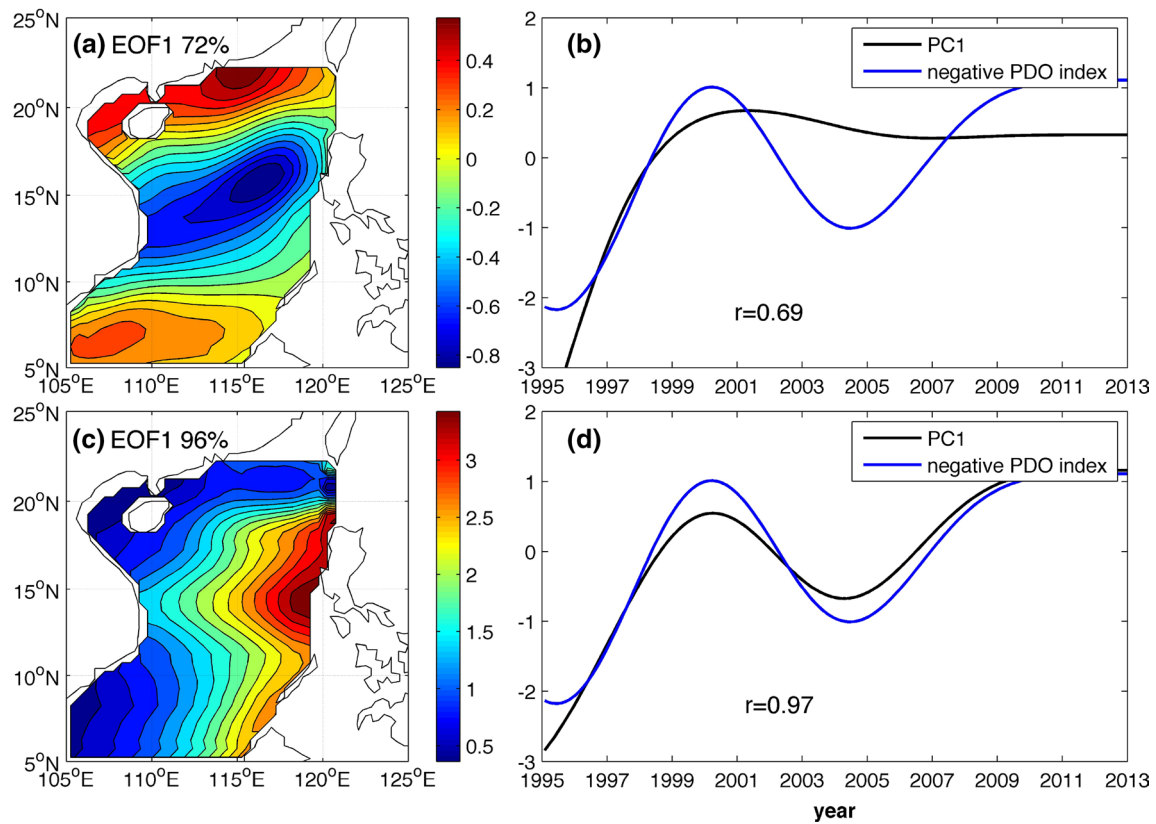


Fig. 11 **a** First EOF pattern of decadal SLA (cm) caused by the wind-driven Rossby waves in the SCS. **b** Corresponding normalized principal component (black curve), normalized 1 negative PDO index

(blue curve). **c, d** Same as **(a)** and **(b)** except for sea-level anomalies forced by the Rossby waves radiated from the eastern boundary

Many studies have suggested that the PDO accounts for a significant part of decadal sea-level variability in the WTP (e.g., Merrifield et al. 2012; Zhang and Church 2012). Merrifield et al. (2012), for example, concluded that the high rate of sea-level rise in the WTP during the last two decades is due to the intensification of the easterly trade winds associated with the PDO (Fig. 10a). The intensified easterly trade winds and negative wind stress curl deepen the thermocline in the WTP, thereby increasing steric and total sea level. In contrast to the western Pacific, the cyclonic wind anomaly potentially forced negative sea-level anomaly in the central SCS during 1993–2012.

3.2.2 Model simulations

We use the 1.5-layer model to investigate decadal adjustment in the SCS. Figure 11a, b present the leading mode of decadal SLA forced only by wind within the SCS, which accounts for 72 % of the total variance. The mode features weak negative SLA in the central basin and positive SLA in the northern and southern SCS, indicating that the wind forcing acts to reduce sea level in the central SCS. Figure 11c, d show the leading mode of decadal SLA in the

model forced only by the sea-level signals from the eastern boundary, accounting for 96 % of the total variance. The mode features high variability west of Luzon Island, and closely resembles the pattern from the altimetric data (Figs. 10a, 11c).

The 1.5-layer model results support the idea that westward-propagating, sea-level signals from the eastern boundary dominate the decadal and long-term variability of SLA in the SCS. Along the west coasts of Borneo and Palawan Islands, the correlation coefficient between along-shore wind stress anomaly and SLA is 0.88 (significant at the 95 % level), indicative of the importance of forcing by alongshore wind (figure not shown). SLA in box A is significantly correlated with that to the southeast of Philippine Archipelago ($r = 0.94$, figure not shown), which supports the idea that sea-level signals along the western coast of Luzon Island originate from the western tropical Pacific.

3.2.3 Analysis back to 1950

The PDO shifts phase usually about every 20–30 years (Mantua et al. 1997). Whether the high correlation still exist between sea level averaged in the SCS and the PDO

Fig. 12 Time series of decadal SLA from the reconstructed data (*black curve*, cm) averaged in the SCS and negative PDO index (*blue curve*). Linear trend is removed from all time series

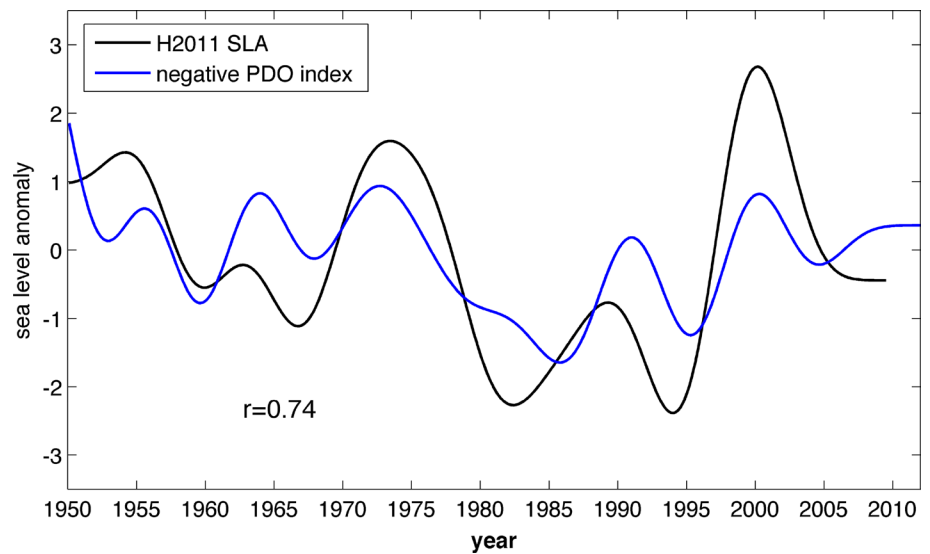
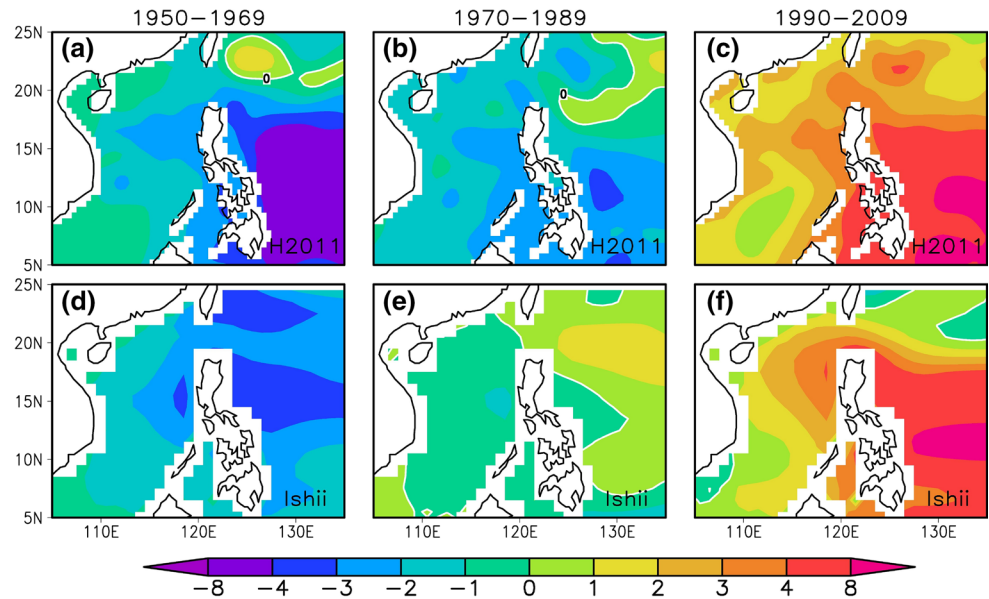


Fig. 13 **a–c** Sea level trends (mm/year) over the SCS and western Pacific from reconstructed data during 1950–1969, 1970–1989, 1990–2009, respectively. **d–f** Same as **(a)–(c)**, except for except for steric sea-level trends from Ishii data. Linear trends during 1950–2009 are removed from time series at each grid point



over a longer period or not merits further examination. Figure 12 presents the decadal sea-level anomaly from the reconstructed data averaged in the SCS from 1950–2009. Mean sea level fell during 1950–1968, and then rose until 1975, reaching a high level. After that, sea level fell again, reaching a lowest level in 1995, and then rose fast during last two decades. The correlation coefficient between mean sea level and negative PDO index reaches its maximum when they are correlated simultaneously ($r = 0.74$, significant at the 95 % level), indicating that the high correlation between sea level in the SCS and the PDO has existed over the last 60 years.

From 1980–1993, the SCS sea level was somewhat out of phase with the PDO. Previous studies indicated that heat advection associated with LST explains the variability of

basin mean heat content and sea level in the SCS to a great extent (Qu et al. 2004; Cheng and Qi 2007). Based on an eddy-resolving OGCM for the Earth Simulator (OFES), Yu and Qu (2013) revealed a good correlation between LST and the PDO index on decadal time scale over the last 60 years. They also noted that the two time series are out of phase during 1980–1993.

The multidecadal variability of the H2011 and thermos-teric sea level are more clearly shown in Fig. 13, which presents the spatial patterns of sea level and steric sea level trends in the SCS and western Pacific during the three periods: period I (1950–1969), period II (1970–1989), period III (1990–2009). To emphasize sea-level trend related only to decadal variability, the long-term trend from 1950 to 2009 has been removed from each grid point. The H2011

sea level shows negative trend in the SCS and western Pacific over period I. The pattern of thermosteric sea level is very similar to that of reconstructed sea level, such as strong variances in the WTP and west of Luzon Island, indicating that thermosteric variability dominates decadal and long-term variability of sea level in the SCS. Over period II, H2011 and thermosteric sea level display weak negative trends in the SCS. The pattern of local sea level trend over period III are opposite to that over period I. Over 1950–2009, sea level trends in the SCS and western Pacific have large-scale multidecadal shift in the early 1990. The consistency among H2011 and thermosteric sea level analyses establishes the utility of reconstructed sea level in the SCS and western Pacific over the past 60 years, and indicates that the PDO had a great impact on the sea-level change in the SCS and the western Pacific over the period.

4 Conclusions and discussion

We have examined interannual-to-decadal variability and long-term trends of sea level in the SCS using 20 years of altimetric observations and reconstructed sea-level data over the past 60 years. The interannual variability of SLA features significant seasonality. In the interior of the SCS, the wind-stress curl anomalies associated with ENSO explain the interannual SLA pattern quite well, with Rossby waves from the eastern boundary contributing to sea-level variability primarily in the eastern SCS. On decadal and longer timescales, strong sea level variability is found west of Luzon Island. Decadal variability of sea level in the SCS follows that in the western Pacific, with both signals being highly correlated with the PDO. Utilizing a 1.5-layer model, we show that in the SCS, Rossby waves propagating from the eastern boundary dominate the decadal variability of sea level in the SCS, with local wind damping the variability in the central SCS.

Figure 14 gives a schematic diagram of remote wave forcing from Northwest Pacific and local wave adjustment on the sea level in the SCS. Sea-level signals from the WTP propagate westward as Rossby waves. When Rossby waves reach east coast of the Philippines, they transform into coastal-trapped waves, propagating clockwise along the coast of the Philippine Archipelago. When signals reach the west coast of Luzon Island, they radiate Rossby waves, which propagate westward and impact on the sea-level variations in the deep basin. In the interior SCS, coastal-trapped waves can propagate anticlockwise around the perimeter of the SCS, bend around the northern tip of Palawan Island and then propagate along the western coast of Sulu Sea. Along the west coast of Borneo and Palawan Islands, no significant wave propagation is found (Fig. 9a, c), which indicates that sea level signals from the western

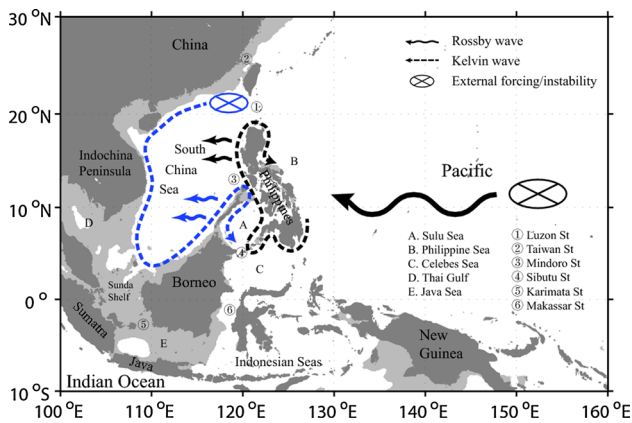
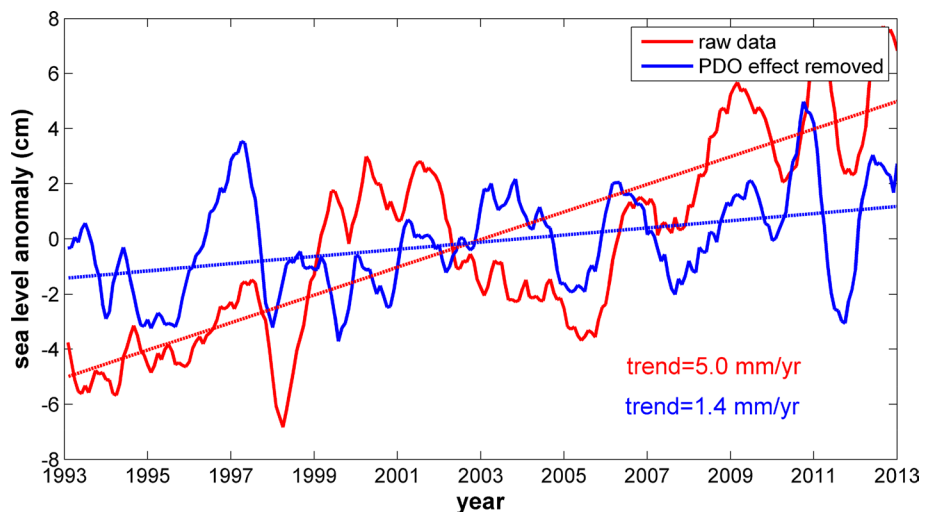


Fig. 14 Schematic diagram of remote wave forcing from Northwest Pacific and local wave adjustment on the sea level in the South China Sea

Fig. 15 Time series of SLA in the South China Sea (red curve, cm) and residual time series after removing PDO correlated variability (blue curve), superimposed the trend lines



and southern shelf are relatively weak and local along-shore wind plays an important role in sea-level fluctuations (Fig. 8b).

Basin-mean sea level in the SCS rose at a rate of 5.0 mm/year during 1993–2012 (Fig. 15). The rate is higher than that of global mean sea level, at 3.3 mm/year from 1993–2010 (Leuliette and Willis 2011). Decadal SLA averaged in the SCS has a significant correlation with the PDO ($r = -0.96$, Fig. 10b), indicating that sea level linear trends for the recent 20 years are greatly affected by the low-frequency variability associated with the PDO. We used a multiple variable linear regression to isolate the impact of PDO on long-term trend of sea level. Figure 15 shows that the PDO contribution to the SCS sea level trend is approximately 3.6 mm/year (about 72 % of total sea-level rise) for the satellite altimetry era (1993–2012). After removing PDO effect, the linear trend decreases to 1.4 mm/year, very close to the sea-level trend for the past 60 years derived from the reconstructed sea level data (1.7 ± 0.1 mm/year, Peng et al. 2013). This agreement suggests that the PDO-corrected sea-level trend more objectively reflects the SCS response to global climate warming, a result that helps improve future projections of sea level rise in the SCS.

The satellite altimeter era coincides with a major phase shift of PDO that took place since the 1990s. This PDO event is associated with the accelerated trade winds on the equator, which pile up warm water and raise sea level in the western tropical Pacific but reduce sea level off the west coast of the Americas (Merrifield et al. 2012). The equatorial trade wind acceleration is coupled with a decadal cooling of the tropical Pacific, which has caused the global mean temperature to stall for the past 15 years (Kosaka and Xie 2013; Dai et al. 2015). Thus, the accelerated sea level rise in the SCS is part of global adjustment to the PDO phase shift.

Acknowledgments We wish to thank Prof. Julian P. McCreary for editing the revised manuscript. This study benefited from discussions with Profs. Bo Qiu and Fei-fei Jin. We are also grateful to two anonymous reviewers whose constructive comments helped improve the manuscript. This work was supported by “Strategic Priority Research Program” of the Chinese Academy of Sciences (XDA11010103), the National Basic Research Program of China (2012CB955603), the Natural Science Foundation of China (41176023, 41276108, 41230962), and the U.S. National Science Foundation. X.H.C is also sponsored by the “Youth Innovation Promotion Association”, CAS (SQ201204, LTOZZ1202) and China Scholarship Council.

References

Chang CWJ, Hsu HH, Wu CR, Sheu WJ (2008) Interannual mode of sea level in the South China Sea and the roles of El Niño and El Niño Modoki. *Geophys Res Lett* 35:L03601. doi:10.1029/2007GL032562

- Chen X, Qiu B, Cheng X, Qi Y, Du Y (2015) Intraseasonal variability of Pacific-originated sea level anomaly around the Philippine Archipelago. *J Oceanogr*. doi:10.1007/s10872-015-0281-9
- Cheng X, Qi Y (2007) Trends of sea level variations in the South China Sea from merged altimetry data. *Global Planet Change* 57:371–382. doi:10.1016/j.gloplacha.2007.01.005
- Cheng X, Qi Y, Zhou W (2008) Trends of sea level variations in the Indo-Pacific warm pool. *Global Planet Change* 63:57–66. doi:10.1016/j.gloplacha
- Church JA, White NJ (2006) A 20th century acceleration in global sea-level rise. *Geophys Res Lett* 33:L01602. doi:10.1029/2005GL024826
- Dai A, Fyfe JC, Xie SP, Dai X (2015) Decadal modulation of global surface temperature by internal climate variability. *Nature Clim Chang*. doi:10.1038/nclimate2605
- Dee DP et al (2011) The ERA-Interim reanalysis: configuration and performance of the data assimilation system. *Quart J Roy Meteor Soc* 137:553–597
- Dibarboure G, Lauret O, Mertz F, Rosmorduc V, Maheu C (2008) SSALTO/DUACS user handbook: (M)SLA and (M)ADT near-real time and delayed time products, Rep. CLS-DOS-NT-06.034, pp39 Aviso Altimetry, Ramonville St. Agne, France
- Du Y, Qu T (2010) Three inflow pathways of the Indonesian through-flow as seen from the simple ocean data assimilation. *Dyn Atmos Oceans* 50(2):233–256
- Du Y, Xie SP (2008) Role of atmospheric adjustments in the tropical Indian Ocean warming during the 20th century in climate models. *Geophys Res Lett* 35:L08712. doi:10.1029/2008GL033631
- Du Y, Yang L, Xie SP (2011) Tropical Indian Ocean influence on Northwest Pacific tropical cyclones in summer following strong El Niño. *J Clim* 24:315–322. doi:10.1175/2010JCLI3890.1
- Fang G, Chen H, Wei Z, Wang Y, Wang X, Li C (2006) Trends and interannual variability of the South China Sea surface winds, surface height, and surface temperature in the recent decade. *J Geophys Res* 111:C11S16. doi:10.1029/2005JC003276
- Fu LL, Qiu B (2002) Low-frequency variability of the North Pacific Ocean: the roles of boundary- and wind-driven baroclinic Rossby waves. *J Geophys Res* 107(C12):3220. doi:10.1029/2001JC001131
- Gordon AL, Huber BA, Metzger EJ, Susanto RD, Hurlburt HE, Adi TR (2012) South China Sea throughflow impact on the Indonesian throughflow. *Geophys Res Lett* 39:L11602. doi:10.1029/2012GL052021
- Hamlington BD, Leben RR, Nerem RS, Han W, Kim KY (2011) Reconstructing sea level using cyclostationary empirical orthogonal functions. *J Geophys Res* 116:C12015. doi:10.1029/2011JC007529
- Han W, Meehl GA, Hu A, Alexander MA, Yamagata T, Yuan D, Ishii M, Pegion PP, Zheng J, Hamlington BD, Quan XW, Leben RR (2013) Intensification of decadal and multi-decadal sea level variability in the western tropical Pacific during recent decades. *Clim Dyn*. doi:10.1007/s00382-013-195-1
- Ishii M, Kimoto M (2009) Reevaluation of historical ocean heat content variations with time-varying XBT and MBT depth bias corrections. *J Oceanogr* 65:287–299. doi:10.1007/s10872-009-0027-7
- Ishii M, Kimoto M, Sakamoto K, Iwasaki SI (2006) Steric sea level changes estimated from historical subsurface temperature and salinity analyses. *J Oceanogr* 62(2):155–170
- Jing Z, Qi Y, Du Y (2011) Upwelling in the continental shelf of northern South China Sea associated with 1997–1998 El Niño. *J Geophys Res* 116:C02033. doi:10.1029/2010JC006598
- Kosaka Y, Xie SP (2013) Recent global-warming hiatus tied to equatorial Pacific surface cooling. *Nature* 501:403–407. doi:10.1038/nature12534
- Lau NC, Wang B (2005) Monsoon-ENSO interactions. In: *The global monsoon system: research and forecast*, Geneva, Switzerland, WMO, WMO/TD No. 1266, TMRP Report No. 70, 299–309

- Lee T, McPhaden MJ (2008) Decadal phase change in large-scale sea level and winds in the Indo-Pacific region at the end of the 20th century. *Geophys Res Lett* 35:L01605. doi:[10.1029/2007GL032419](https://doi.org/10.1029/2007GL032419)
- Leuliette EW, Willis JK (2011) Balancing the sea level budget. *Oceanography* 24(2):122–129. doi:[10.5670/oceanog.2011.32](https://doi.org/10.5670/oceanog.2011.32)
- Li L, Xu J, Cai R (2002) Trends of sea level rise in the South China Sea during the 1990s: an altimetry result. *Chin Sci Bull* 47(7):582–585
- Liu Z, Yang H, Liu Q (2001) Regional dynamics of seasonal variability in the South China Sea. *J Phys Oceanogr* 31:272–284
- Liu Q, Feng M, Wang D (2011) ENSO-induced interannual variability in the southeastern South China Sea. *J Oceanogr* 67:127–133. doi:[10.1007/s10872-011-0002-y](https://doi.org/10.1007/s10872-011-0002-y)
- Luo J, Sasaki W, Masumoto Y (2012) Indian Ocean warming modulates Pacific climate change. *Proc Natl Acad Sci USA* 109(46):18701–18706
- Mantua NJ, Hare SR, Zhang Y, Wallace JM, Francis RC (1997) A Pacific interdecadal climate oscillation with impact on salmon production. *Bull Am Meteorol Soc* 78(6):1069–1079. doi:[10.1175/1520-0477\(1997\)078<1069:APICOW>2.0.CO;2](https://doi.org/10.1175/1520-0477(1997)078<1069:APICOW>2.0.CO;2)
- Merrifield MA, Thompson PR, Lander M (2012) Multidecadal sea level anomalies and trends in the western tropical Pacific. *Geophys Res Lett* 39:L13602. doi:[10.1029/2012GL052032](https://doi.org/10.1029/2012GL052032)
- Metzger EJ, Hurlburt H (1996) Coupled dynamics of the South China Sea, the Sulu Sea, and the Pacific Ocean. *J Geophys Res* 101:12331–12352
- Nidheesh A, Lengaigne M, Vialard J, Unnikrishnan A, Dayan H (2012) Decadal and long-term sea level variability in the tropical Indo-Pacific Ocean. *Clim Dyn* 41:381–402. doi:[10.1007/s00382-012-1463-4](https://doi.org/10.1007/s00382-012-1463-4)
- Peng D, Palanisamy H, Cazenave A, Meyssignac B (2013) Interannual sea level variations in the South China Sea Over 1950–2009. *Mar Geod* 36(2):164–182. doi:[10.1080/01490419.2013.771595](https://doi.org/10.1080/01490419.2013.771595)
- Qiu B (2002) Large-scale variability in the midlatitude subtropical and subpolar North Pacific Ocean: observations and causes. *J Phys Oceanogr* 32:353–375
- Qu T (2000) Upper layer circulation in the South China Sea. *J Phys Oceanogr* 30:1450–1460
- Qu T, Kim YY, Yaremchuk M, Tozuka T, Ishida A, Yamagata T (2004) Can Luzon Strait transport play a role in conveying the impact of ENSO to the South China Sea? *J Clim* 17:3644–3657. doi:[10.1175/1520-0442017<3644:CLSTPA>2.0.CO;2](https://doi.org/10.1175/1520-0442017<3644:CLSTPA>2.0.CO;2)
- Qu T, Du Y, Sasaki H (2006) South China Sea throughflow: a heat and freshwater conveyor. *Geophys Res Lett* 33:L23617. doi:[10.1029/2006GL028350](https://doi.org/10.1029/2006GL028350)
- Rong Z, Liu Y, Zong H, Cheng Y (2007) Interannual sea level variability in the South China Sea and its response to ENSO. *Global Planet Change* 55:257–272. doi:[10.1016/j.gloplacha.2006.08.001](https://doi.org/10.1016/j.gloplacha.2006.08.001)
- Volkov DL, Larnicol G, Dorandeu J (2007) Improving the quality of satellite altimetry data over continental shelves. *J Geophys Res* 112:C06020. doi:[10.1029/2006JC003765](https://doi.org/10.1029/2006JC003765)
- Wang B, An SI (2005) A method for detecting season-dependent modes of climate variability: S-EOF analysis. *Geophys Res Lett* 32:L15710. doi:[10.1029/2005GL022709](https://doi.org/10.1029/2005GL022709)
- Wang B, Wu R, Fu X (2000) Pacific-East Asian teleconnection: how does ENSO affect East Asian climate? *J Clim* 13:1517–1536. doi:[10.1175/1520-0442013<1517:PEATHD>2.0.CO;2](https://doi.org/10.1175/1520-0442013<1517:PEATHD>2.0.CO;2)
- Wang G, Chen D, Su J (2006) Generation and life cycle of the dipole in South China Sea summer circulation. *J Geophys Res Oceans* 111:C06002. doi:[10.1029/2005JC003314](https://doi.org/10.1029/2005JC003314)
- Wang G, Wang C, Huang RX (2010) Interdecadal variability of the eastward current in the South China Sea associated with the summer Asian monsoon. *J Clim* 23:6115–6123. doi:[10.1175/2010JCLI3607.1](https://doi.org/10.1175/2010JCLI3607.1)
- Wang T, Du Y, Zhuang W, Wang J (2015) Connection of sea level variability between Tropical Western Pacific and Southern Indian Ocean during recent two decades. *Sci China D*. doi:[10.1007/s11430-014-5048-4](https://doi.org/10.1007/s11430-014-5048-4)
- Wu J (1982) Wind-stress coefficients over sea surface from breeze to hurricane. *J Geophys Res* 87(12):9704–9706
- Wu CR (2013) Interannual modulation of the Pacific Decadal Oscillation (PDO) on the low-latitude western North Pacific. *Prog Oceanogr* 110:49–58. doi:[10.1016/j.pocean.2012.12.001](https://doi.org/10.1016/j.pocean.2012.12.001)
- Wu CR, Chang CWJ (2005) Interannual variability of the South China Sea in a data assimilation model. *Geophys Res Lett* 32:L17611. doi:[10.1029/2005GL023798](https://doi.org/10.1029/2005GL023798)
- Xie SP, Xie Q, Wang DX (2003) Liu WT (2003) Summer upwelling in the South China Sea and its role in regional climate variations. *J Geophys Res Oceans* 108:3261
- Xie SP, Hu K, Hafner J, Tokinaga H, Du Y, Huang G, Sampe T (2009) Indian Ocean capacitor effect on Indo-western Pacific climate during the summer following El Niño. *J Clim* 22(3):730–747. doi:[10.1175/2008JCLI2544.1](https://doi.org/10.1175/2008JCLI2544.1)
- Xie SP, Du Y, Huang G, Zheng XT, Tokinaga H, Hu K, Liu Q (2010) Decadal shift in El Niño influences on Indo-western Pacific and East Asian climate in the 1970s. *J Clim* 23(12):3352–3368
- Yang JL, Liu QY, Xie SP, Liu ZY, Wu LX (2007) Impact of the Indian Ocean SST basin mode on the Asian summer monsoon. *Geophys Res Lett* 34:L02708. doi:[10.1029/2006GL028571](https://doi.org/10.1029/2006GL028571)
- Yu K, Qu T (2013) Imprint of the Pacific Decadal Oscillation on the South China Sea throughflow variability. *J Clim* 26(24):9797–9805. doi:[10.1175/JCLI-D-12-00785.1](https://doi.org/10.1175/JCLI-D-12-00785.1)
- Zhang X, Church JA (2012) Sea level trends, interannual and decadal variability in the Pacific Ocean. *Geophys Res Lett* 39:L21701. doi:[10.1029/2012GL053240](https://doi.org/10.1029/2012GL053240)
- Zhuang W, Feng M, Du Y, Schiller A, Wang D (2013a) Low-frequency sea level variability in the southern Indian Ocean and its impacts on the oceanic meridional transports. *J Geophys Res Oceans* 118:1302–1315. doi:[10.1002/jgrc.20129](https://doi.org/10.1002/jgrc.20129)
- Zhuang W, Qiu B, Du Y (2013b) Low-frequency western Pacific Ocean sea level and circulation changes due to the connectivity of the Philippine Archipelago. *J Geophys Res Oceans* 118:6759–6773. doi:[10.1002/2013JC009376](https://doi.org/10.1002/2013JC009376)